

01 Mar 2008

Automatic Drift Compensation Using Phase Correlation Method for Nanomanipulation

Qinmin Yang


Jagannathan Sarangapani

Missouri University of Science and Technology, sarangap@mst.edu

Eric W. Bohannon

Missouri University of Science and Technology, bohannon@mst.edu

Follow this and additional works at: https://scholarsmine.mst.edu/ele_comeng_facwork

 Part of the [Computer Sciences Commons](#), and the [Electrical and Computer Engineering Commons](#)

Recommended Citation

Q. Yang et al., "Automatic Drift Compensation Using Phase Correlation Method for Nanomanipulation," *IEEE Transactions on Nanotechnology*, Institute of Electrical and Electronics Engineers (IEEE), Mar 2008. The definitive version is available at <https://doi.org/10.1109/TNANO.2007.915021>

This Article - Journal is brought to you for free and open access by Scholars' Mine. It has been accepted for inclusion in Electrical and Computer Engineering Faculty Research & Creative Works by an authorized administrator of Scholars' Mine. This work is protected by U. S. Copyright Law. Unauthorized use including reproduction for redistribution requires the permission of the copyright holder. For more information, please contact scholarsmine@mst.edu.

Automatic Drift Compensation Using Phase Correlation Method for Nanomanipulation

Qinmin Yang, *Student Member, IEEE*, S. Jagannathan, *Senior Member, IEEE*, and E. W. Bohannon

Abstract—Nanomanipulation and nanofabrication with an atomic force microscope (AFM) or other scanning probe microscope (SPM) are a precursor for nanomanufacturing. It is still a challenging task to accomplish nanomanipulation automatically. In ambient conditions without stringent environmental controls, the task of nanomanipulation requires extensive human intervention to compensate for the spatial uncertainties of the SPM. Among these uncertainties, the thermal drift, which affects spatial resolution, is especially hard to solve because it tends to increase with time, and cannot be compensated simultaneously by feedback from the instrument.

In this paper, a novel automatic compensation scheme is introduced to measure and estimate the drift one-step ahead. The scheme can be subsequently utilized to compensate for the thermal drift so that a real-time controller for nanomanipulation can be designed, as if the drift did not exist. Experimental results show that the proposed compensation scheme can predict drift with a small error, and therefore, can be embedded in the controller for manipulation tasks.

Index Terms—Nanomanipulation, neural network (NN), phase correlation method, scanning probe microscope, thermal drift.

I. INTRODUCTION

NANOMANIPULATION, which aims at manipulating nanometer size objects with nanometer precision, has become possible since 1990 [1] after the invention of scanning tunneling microscopes (STM), atomic force microscopes (AFM), and other types of scanning probe microscopes (SPMs). By accurately controlling atoms, molecules, or nanoscale objects, numerous applications of nanotechnology can be cited in the area of molecular biology and genetics, solid-state physics, chemistry, material science, computer industry, and medicine. By reducing the object size from micrometer to nanometer, new sensors, terabyte capacity memories, deoxyribonucleic acids (DNA) computers, man-made materials, etc., would be possible within the near future [2].

Today, the manipulation of particles with the order of 10 nm in diameter using AFMs is being investigated by many researchers [3], [10]–[13], [17]. Preliminary controller designs

Manuscript received November 8, 2006; revised May 28, 2007. This work was supported in part by the National Science Foundation (NSF) under Grant ECCS#0621924 and in part by the Intelligent Systems Center. The review of this paper was arranged by Associate Editor M. Freeman.

Q. Yang and S. Jagannathan are with the Department of Electrical and Computer Engineering, University of Missouri–Rolla, Rolla, MO 65409 USA (e-mail: qyy74@umr.edu; sarangap@mst.edu).

E. W. Bohannon is with the Materials Research Center, University of Missouri–Rolla, Rolla, MO 65409 USA (e-mail: Bohannon@mst.edu).

Color versions of one or more of the figures in this paper are available online at <http://ieeexplore.ieee.org>.

Digital Object Identifier 10.1109/TNANO.2007.915020

for nanomanipulation systems were introduced in [14] and [15]. Besides using AFM or other SPM as imaging tools, they are also employed as teleoperated manipulators at the nano scale. However, for future new nanotechnology products, there are still many challenges to be addressed. From macro to nano world, any nonlinearity such as thermal noise, even if it is small, will cause major hurdles during manipulation with the microscope. Without treating these uncertainties, real-time controller designs will be impractical. Therefore, at present, the nanomanipulation requires extensive user intervention to compensate for the spatial uncertainties associated with the microscope and its piezoelectric drive mechanism, such as hysteresis, creep, and thermal drift [3], [16], [17], when operated in ambient conditions without stringent environmental controls.

Among the uncertainties that AFM encounters, hysteresis can be reduced by scanning in the same direction always, while creep effects almost vanish by waiting a few minutes after a large scanning motion [3]. Alternatively, a comprehensive study is presented in [16] on techniques that are being developed to compensate them. Usually, these solutions are normally embedded into an AFM software for compensation although they slow down the manipulation tasks.

Nevertheless, unlike other uncertainties, the effect of the drift will increase with time, and it cannot be compensated automatically by the instrument. In other words, due to the temperature change in the ambient environment, the AFM tip drifts with time at a speed of about one atomic diameter per second, even when the voltage inputs for controlling the tip position are held constant. Although the drift can be greatly reduced by placing the microscope in a temperature-controlled and ultrahigh vacuum (UHV) environment, this will be expensive and difficult, and therefore, will limit its applications in the industry. At the same time, other uncertainties such as calibration error and instrument noise will be introduced during the manipulation processes, and their effects are similar to that of the thermal drift that renders gross manipulation inaccuracies. As a result, it will typically take hours for an experienced operator to construct a pattern with several nanoparticles using the AFM. To efficiently and successfully accomplish such tasks or even more complex ones, an automated manipulation is desirable. For an automated nanomanipulation, the drift compensation is the first step.

Several researchers have addressed the problem of drift and proposed solutions in [3] through [8] and [17]. However, most of them [4]–[8] are assuming that the drift is held at a constant value. Additionally, in [4]–[8], the drift is computed by considering the entire image data, although during manipulation, part of topography of the sample is changed. To overcome this problem, in this paper, a block-based phase correlation method

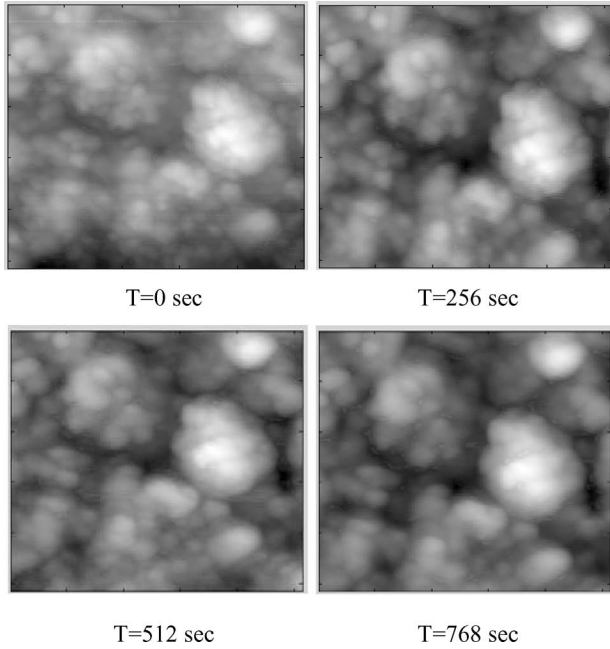


Fig. 1. Image sequences of a graphite sample taken at 256 s intervals by an AFM showing drift on the x - y plane due to ambient conditions. The scanned area is $512 \times 512 \text{ nm}^2$.

is employed to divide the entire image into blocks, using which drift for each block is estimated individually. Thereafter, the drift value of the entire image is computed based on the drift calculation for each block.

Further, to make this method suitable for future real-time controller design, both a neural network (NN) and signal reconstruction technique are also necessary and proposed here. As a matter of fact, given diverse working conditions during manipulation, an artificial NN is utilized for predicting drift at the next sampling interval for relaxing the need for drift models. Using signal reconstruction techniques, the drift can be expressed as a continuous function of time for any real-time controller design.

The paper is organized as follows. In Section II, the problem of drift is introduced, whereas Section III presents the detailed compensation methodology for the drift problem. The system implementation and experimental results are included in Section IV before conclusions.

II. PROBLEM STATEMENT

Mainly due to the thermal expansion and the contraction of the microscope components and the sample in ambient conditions, drift usually appears in successive AFM scans even when all of the scanning parameters are not altered. In the x - y plane (or the horizontal plane), drift can be observed as a translation between different images, as shown in Fig. 1. The drift velocities on the x - y plane are reported to vary from 0.01 to 0.1 nm/s [3]. However, during our experiments, the problem due to drift appears to be worse at times. As observed from Fig. 1, the graphite sample is drifting to the left at a speed of around 0.5 nm/s. So, the drift between any two images taken at a 256 s interval can be as much as 128 nm, which is larger than the diameter of the

nanoparticles themselves that are normally manipulated. Meanwhile, from the height data of the sample, it can be observed that the drift along the z -direction is approximately 0.005 nm/s during our experiments.

Unfortunately, measuring drift precisely in the z -direction will be difficult or impossible because the topographic data provided by an SPM are essentially relative height information in terms of discrete points on the sample surface. Fortunately, considering that the vertical drift is comparatively small and has little impact on the controller [3], there is no need to estimate its exact value. In fact, the effect of vertical drift can be mitigated by using gradient images, as will be introduced later. Thus, it is normally sufficient for a drift compensation scheme to estimate and compensate the drift along the x - and y -directions and under the reduced influence of the noise from the z -axis, so that the automated nanomanipulation can be performed as if the drift does not exist.

Past experiments show that the drift along x - and y -directions can be observed as a translational movement and not as a rotation [3], [17]. Furthermore, there is a negligible correlation between the two directions [3]. Hence, ideally, the height data between the two consecutive collections along with the drift can be written as

$$h_{k+1}(x, y) = h_k(x + \Delta x_k, y + \Delta y_k) + \Delta z_k \quad (1)$$

where Δx_k , Δy_k , and Δz_k denote the drift in the x -, y -, and z -axes, respectively, between time instants k and $k + 1$. Here, we assume that every point of the overall imaging area of the sample has the same drift value along the z -direction, which appears to be a reasonable assumption.

Although several methods [4]–[8] to compensate for the drift in the horizontal plane have been proposed, these techniques fail to provide accurate compensation when the drift velocity changes, as illustrated by the experimental results in Fig. 1. A novel Kalman-filter-based estimator [3] and compensator is introduced. However, the user still has to select the appropriate model parameters for every experiment, which will be very difficult for automation. Moreover, the techniques in [3]–[8] are based on comparing successive images of an unmodified sample or unmodified part of the sample. Unfortunately, the topography in the scanning region is usually changed during manipulation or fabrication processes. For instance, as shown in Fig. 2, there are two particles being pushed by the operator, and it is not too difficult to notice that a drift exists between the two images. Under this condition, the methods reported in [4]–[8] render inaccurate results. The tracking window technique can solve this problem, but it is not a true automatic approach.

In this paper, drift will be measured and processed using block-based phase correlation method in a totally automatic manner, and without human intervention, and even when some areas of the sample have been altered due to manipulation.

III. COMPENSATION METHODOLOGY

The block diagram of the proposed compensation methodology is depicted in Fig. 3. The entire system will operate in a recursive fashion with a constant sampling interval, where

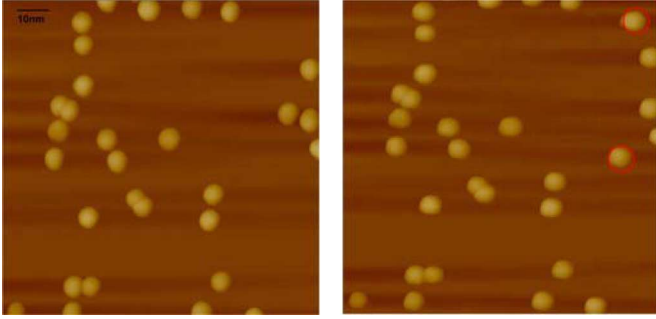


Fig. 2. Image sequences of gold particles with 30 nm diameter on the mica substrate with manipulation under an AFM for the scanned area of $1024 \times 1024 \text{ nm}^2$. Note: There are two particles at the right top corner moved by the operator (one is pushed into the image from outside and the other is moved downwards). Drift also present upside.

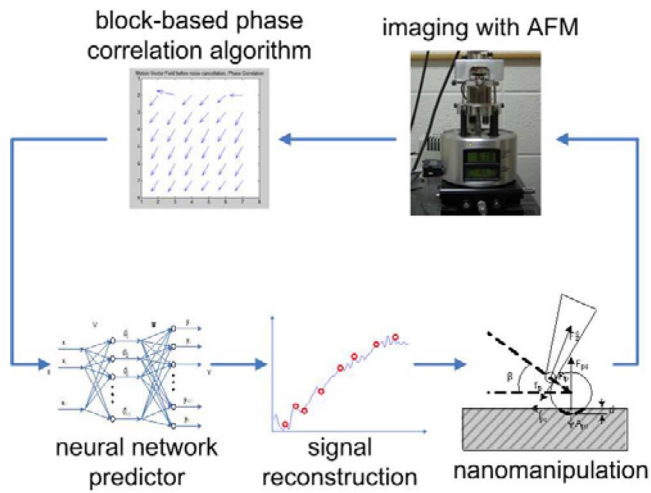


Fig. 3. Block diagram of the overall proposed drift compensation system.

images of the sample are secured by the microscope. Our drift compensator is updated even when the manipulation is carried out elsewhere on the sample during the interimaging period, which is the case discussed in [4]–[8].

The entire manipulation scheme will be executed by the following procedure in a recurrent manner. Once the microscope acquires a most up-to-date image data, the block-based phase correlation algorithm starts and computes a measurement of the current drift value. As soon as this computation is done, it delivers the measurement to the NN predictor. The NN predictor estimates the drift for the next imaging instant, which, in turn, is employed by the signal reconstruction block to form a continuous variation of drift as a function of time between the current imaging instant and the next one. With the drift information expressed as a continuous function of time, the task of nanomanipulation can be accomplished automatically by the controller, as the drift estimate can be explicitly utilized during nanomanipulation.

As stated earlier, there is no correlation between the drift along x - and y -axes [3]. Therefore, for simplicity, only the drift in the x -direction is discussed in the following sections, and the drift in the y -direction can be obtained similarly, and therefore, omitted.

A. Gradient Imaging

In principle, an AFM operates by measuring attractive or repulsive forces between the tip and the sample surface. As a raster-scan drags the tip over the sample, some sort of detection apparatus (e.g., laser) tracks the forces by monitoring the vertical deflection of the AFM cantilever, which indicates the height of the sample locally. Thus, the images provided by an AFM are essentially the height data of the sample locally.

It is important to note that the drift in the z -direction depends upon the measurement errors from the x - and y -directions. Although it is comparatively small and has little impact on nanomanipulation, it could still influence the accuracy of our drift algorithm. Therefore, to minimize this error, the gradient information will be used for measuring drift, which is defined as

$$g_k(x, y) = h_k(x, y) - h_k(x - 1, y). \quad (2)$$

From (2), one can find that a new image is formed by using the gradient information and by just taking the height difference between each pixel and the corresponding horizontal neighboring pixel in the original image. This is also called the horizontal gradient image. The vertical gradient image can be defined similarly, and it is also applicable for our approach. In this paper, only the horizontal gradient is discussed.

Considering the drift factor and substituting (1) into (2) yields

$$\begin{aligned} g_{k+1}(x, y) &= h_{k+1}(x, y) - h_{k+1}(x - 1, y) \\ &= h_k(x + \Delta x_k, y + \Delta y_k) + \Delta z_k \\ &\quad - (h_k(x + \Delta x_k - 1, y + \Delta y_k) + \Delta z_k) \\ &= g_k(x + \Delta x_k, y + \Delta y_k) \end{aligned} \quad (3)$$

where the effect of the z -axis drift is eliminated. Moreover, as observed in our experiments, results using gradient-based images will yield more accurate results than using the original height data due to the presence of the drift along the z -axis. Once the microscope finishes the sample imaging and the gradient calculation, the gradient data is forwarded to the phase correlation module.

B. Block-Based Phase Correlation Method

The drift measurement problem is similar to the motion estimation (ME) and compensation (MC) issue in the area of signal processing. Among various techniques, phase correlation technique measures the motion directly from the image, so that it can give a more accurate and robust estimate of the motion vector and a motion field with a much lower entropy [9]. Additionally, the phase correlation method is computationally very efficient, which will allow more time for manipulation operations between imaging instants. In particular, this method shows a better performance on translational and large-scale motion and these are the characteristics that are normally observed in the AFM drift.

On the other hand, as we argued in the former section, existing methods [3]–[7] will produce inaccurate results in the presence of topography changes of the sample surface resulting from the manipulation, or they need human intervention to mark them manually [8]. In our algorithm, to distinguish the drift from other user-defined operations and further eliminate the drift

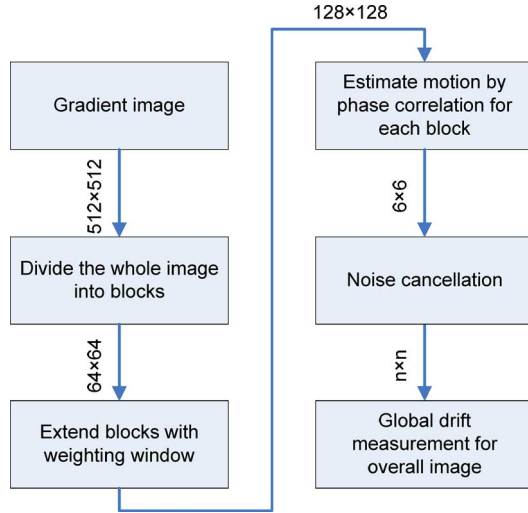


Fig. 4. Schematic diagram of the block-based phase correlation method.

automatically, the image is divided into blocks, and the drift calculation is performed for each block separately. As a matter of fact, block-based motion estimation and compensation schemes are quite popular in practice due to their robust performance, and they do not require object identification. Moreover, they allow some objects in the image to be moved while not influencing the motion estimation of other blocks. This feature makes it easier to estimate the drift of the overall image even when some parts of the sample surface have been altered by operators, which is usually the case in the nanomanipulation environments.

The schematic diagram of our block-based phase correlation method and the parameters used in our experiments are depicted in Fig. 4. Other settings may also be possible for different experimental conditions.

In the proposed scheme, assuming a new gradient frame with 512×512 pixels is received from the AFM, it is first divided into 64×64 pixel blocks. By using a straightforward calculation, there will be 64 blocks from a 512×512 image. The objective of the first step is to estimate the drift value for each block by comparing the new image with the previous one. For more accurately estimating the cross correlation of corresponding block pairs in respective image frames, we extend the blocks to 128×128 pixel in size, centered around the formerly defined 64×64 pixel blocks for calculation. It can be readily found that, with bigger blocks, the overlapping area between the block pair is larger. Therefore, their correlation can still be kept high even with a large amount of drift.

Subsequently, a 2-D raised cosine weighting window is applied to each 128×128 extended block to enforce more weight on our formerly defined 64×64 region. The 2-D raised cosine window is defined as

$$w(x, y) = w_x w_y$$

$$= \frac{1}{4} \left[1 - \cos\left(\frac{2\pi(x+1/2)}{M}\right) \right] \left[1 - \cos\left(\frac{2\pi(y+1/2)}{M}\right) \right]$$

for $x, y = 1, 2, \dots, M$ (4)

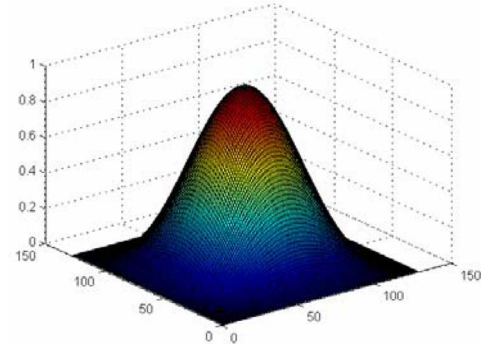


Fig. 5. 2-D raised cosine window function.

where M is the size of the image, which is equal to 128 for our system. The raised cosine function is also illustrated in Fig. 5, which clearly demonstrates that the pixels in the center are given higher emphasis.

Thereafter, the phase correlation method measures the movement between two blocks directly from their phase values. The basic principle is briefly discussed next.

Assume that there exists a translational shift between frames k and $k+1$. In this paper, the same relationship stands for consecutive gradient images, which can be rewritten from (3) as

$$g_{k+1}(x, y) = g_k(x + \Delta x, y + \Delta y). \quad (5)$$

Taking 2-D Fourier transform of (5) yields

$$G_{k+1}(f_x, f_y) = G_k(f_x, f_y) \exp[j2\pi(\Delta x f_x + \Delta y f_y)]. \quad (6)$$

Therefore, the displacement in the spatial domain is reflected as a phase change in the frequency spectrum domain. Further, the cross correlation between any two frames can be written as

$$c_{k,k+1}(x, y) = g_{k+1}(x, y) g_k^*(-x, -y) \quad (7)$$

whose Fourier transform is given by

$$C_{k,k+1}(f_x, f_y) = G_{k+1}(f_x, f_y) G_k^*(f_x, f_y). \quad (8)$$

After normalizing the cross-power spectrum by its magnitude and eliminating the luminance variation influence during our phase analysis, we obtain its phase as

$$\Phi[C_{k,k+1}(f_x, f_y)] = \frac{G_{k+1}(f_x, f_y) G_k^*(f_x, f_y)}{|G_{k+1}(f_x, f_y) G_k^*(f_x, f_y)|}. \quad (9)$$

By substituting (6) into (9), we have

$$\Phi[C_{k,k+1}(f_x, f_y)] = \exp[-j2\pi(\Delta x f_x + \Delta y f_y)] \quad (10)$$

whose 2-D inverse Fourier transform is given by

$$c_{k,k+1}(x, y) = \delta(x - \Delta x, y - \Delta y) \quad (11)$$

where δ is an impulse function on the x - y plane. As a result, the displacement in the spatial domain corresponds to an impulse in the correlation domain. Therefore, by finding the location of the impulse in (11), we are able to obtain an estimate of the displacement, which is represented by a motion vector. In our system, the phase correlation for each block pair in consecutive frames is calculated using 128×128 fast Fourier transform (FFT).

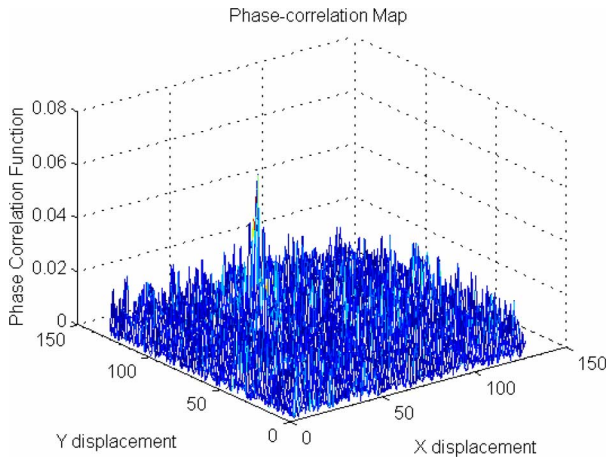
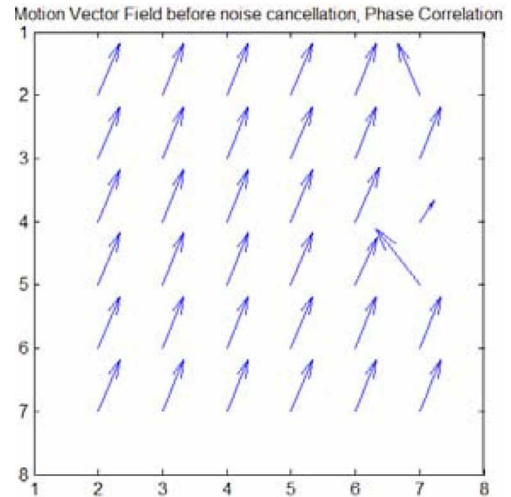


Fig. 6. Map of a typical phase correlation function between two blocks.

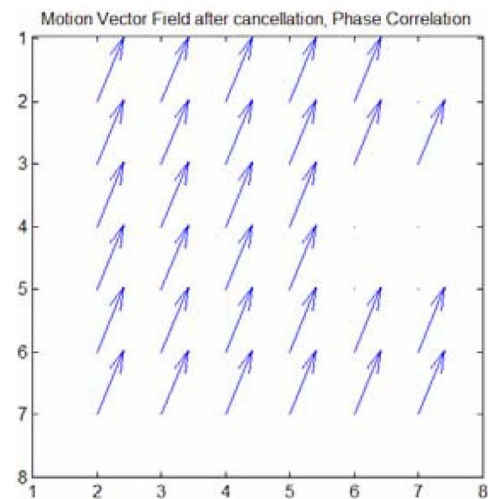
In practice, since the motion between any two blocks cannot be both pure translational and noise-free, usually we have a phase correlation map similar to what is depicted in Fig. 6. Although there is an obvious peak appearing, there are other peaks also, and some with noise.

In other words, in ideal situations where there is only a spatial shift between images due to drift, it should be reflected as a single spike after the application of the phase correlation technique. Therefore, the highest peak in the phase correlation map usually corresponds to the actual drift value. Even if the images are contaminated with noise, the highest peak still provides the best estimate of drift between two frames. However, for our 128×128 pixel extended blocks, due to the nontranslational movement and other unexpected noise, several peaks with height closer to one another might be appearing in the correlation map. In this case, several candidates will be selected first instead of just choosing the highest peak. Thereafter, the peak that best represents the displacement vector for the object block has to be found by examining the peaks using image correlation in terms of the mean squared error (MSE) criterion. The candidate possessing the highest image correlation is then identified, and its corresponding drift displacement is accepted as the motion vector for the object block. Note that a maximum drift of ± 64 pixels is assumed in order to ensure that there exists an overlapping area with enough size between the corresponding block pair. In case the drift exceeds the assumption, one may increase the block size to 128×128 to solve this problem.

Finally, after the motion vectors for all blocks are computed, we could obtain a motion vector as a field map shown in Fig. 7, which is the result of applying our algorithm on the experiment data shown in Fig. 2. Ideally, if the translational drift is the only reason for the motion vectors within the image sequence, a satisfactory drift measurement of the whole frame can be produced by simply calculating the mean of all motion vectors. However, as we have stated before, to fulfill nanomanipulation, some particles or some parts of the sample surface are designed to be altered. Additionally, image data are usually corrupted by noise and other uncertainties at the nanoscale. As a result, some of the blocks will have considerably different motion vector



(a)



(b)

Fig. 7. (a) Motion vector field corresponding to Fig. 2 before the noise cancellation. (b) Motion vector field after the noise cancellation.

values from others, as shown in Fig. 7(a). Thus, a specific noise cancellation mechanism is required to pick the “contaminated” blocks out, and restrain them from being involved into the final calculation.

By assuming that only a limited area of the sample is altered during a short interval, a simple but an effective approach to remove this noise is to first compute the mean of all motion vectors, pick some blocks that are farthest from the mean, and set their values invalid. By this way, a more accurate drift measurement can be obtained by computing the mean of motion vectors of the left blocks.

In practice, a constant threshold value of ε is used in our scheme for noise cancellation. In particular, after getting the mean, all the blocks whose distance to this mean value larger than ε are not considered in the final calculation of the drift measurement for the overall image. Usually, the choice of ε depends on how large area of the sample is being manipulated, which should be known *a priori*.

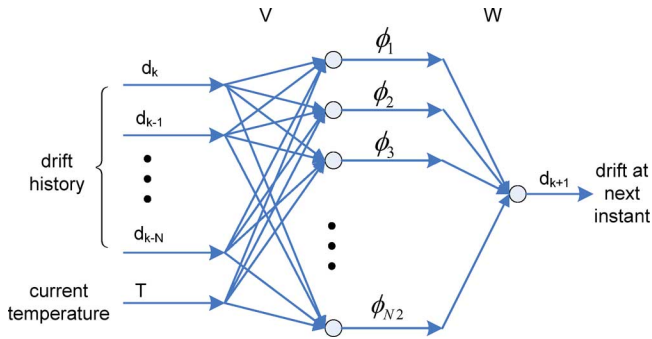


Fig. 8. Architecture of the two-layer NN predictor.

C. Time Series Prediction With NNs

After obtaining the drift measurement at the current time instant k , the drift behavior in the next time-step $k + 1$ must be estimated for compensation purpose. In [3], the Kalman-filter-based estimator is introduced for this purpose. Although Kalman filters can provide the best estimation based on the maximum-likelihood optimization, the model and parameters used in the filter have to be identified beforehand, where a general model and parameter settings are still impossible under multifarious sample materials and varying ambient conditions.

As an alternative, in this paper, a two-layer NN is employed for predicting the drift in the subsequent time instant, as shown in Fig. 8. The matrices V and W are the hidden layer and output layer weights. Moreover, as noticed from Fig. 8, the number of nodes in the input, hidden, and output layers are $N + 1$, N_2 , and 1, respectively, where N denotes the history data utilized in the calculations. It is well known that the NNs have excellent approximation capability for any nonlinear temporal mapping. Assuming that the environmental conditions will not change much in a short-time period, the NNs can learn the statistical nature of the drift from the historical data and other information. In our system, not only the previous drift measurements are forwarded to the NN predictor, but also the temperature fluctuations are measured and taken as an additional input to the NN. The weights of the NN are updated in a supervised training mode along with the drift measurement feedback from the phase correlation algorithm.

D. Signal Reconstruction Using the Sinc Function

For a real-time controller design, it is necessary to obtain a drift description as a continuous function of time from the discrete measured points. Considering that the power spectra of the time series for drift exhibits a bandwidth of the order of 0.001 Hz [3], it is possible to get proper reconstruction results using the sinc function, as long as the sampling interval between the images are small enough. In our applications, the samples are imaged every 256 s or the sampling frequency is about 0.004 Hz. Therefore, it is reasonable to use the sinc function to reconstruct the drift signal without much loss of information.

Therefore, it follows that

$$d(t) = \sum_{i=0}^{k+1} d_i \operatorname{sinc} \left(\frac{\pi(t - t_i)}{\Delta t} \right), \quad \text{for } t \in (t_k, t_{k+1}) \quad (12)$$

where $d(t)$ is the continuous drift function at the time between the current sampling instant to the next one, d_i is the drift measurement ($i = 0, 1, \dots, k$) or prediction ($i = k + 1$) on the sampling time t_i , and Δt is the sampling interval.

IV. IMPLEMENTATION AND EXPERIMENT RESULTS

To verify our proposed research, the drift compensator is implemented on a multimode SPM with NanoScope IIIa controller (Veeco Instruments) at the University of Missouri–Rolla (UMR)’s Materials Research Center. The laboratory has air conditioning but the ambient temperature is not tightly controlled. Additionally, no humidity control is provided in the laboratory. The AFM is forced to operate in tapping mode.

In our experiments, the imaging frequency is set at 0.004 Hz, which implies that each recursive loop of our system takes about 256 s. As a matter of fact, the imaging frequency could be altered. Smaller frequency leads to longer loop period, and therefore, longer manipulation time. However, larger drift volume will be accumulated resulting in degraded experiment outcomes. Meanwhile, the samples are imaged at a scan rate of 4 Hz in our trial. At each scanning, a 512×512 pixel height image representing $1 \mu\text{m}^2$ area is obtained. This means that it takes the AFM about 128 s to finish one imaging routine. Thus, almost half of the loop time can be used for algorithm computation, manipulation, fabrication, and other tasks on the sample. Typically, the computing time of our algorithm is about 15 s on a Pentium M 1.86 GHz computer with 1.00 GB RAM. This means that most of the time can be allocated for manipulation and or fabrication operations, since the computation time is small compared to the imaging time.

For the NN-based drift predictor, a fixed time window of past eight drift measurement values were fed into the input layer of the NN ($N = 8$). The laboratory temperature information is also collected by a thermal sensor attached to the head of the microscope and fed as an additional NN input. The two-layer NN consists of $N_2 = 50$ neurons in the hidden layer. The initial weights of all the layers are selected at random between $[0, 1]$. The activation functions of the first layer are selected as hyperbolic tangent sigmoid functions, and that of the second layer are taken as pure linear functions. Initially, the first 20 sets of drift measurement data will be used for offline training by using the Levenberg–Marquardt backpropagation algorithm. After that, along with the accumulating new measurement data from the phase correlation algorithm block, online learning is utilized by using the training set with the most recent 50 data points.

First, we applied our system on the same sample depicted in Fig. 1. In this experiment, no manipulation work is executed on the sample surface. With the compensator, the AFM is able to focus on the same location as shown in Fig. 9.

The second experiment is taken with a sample of Au on the mica substrate for a duration of 8 h in order to test the feasibility

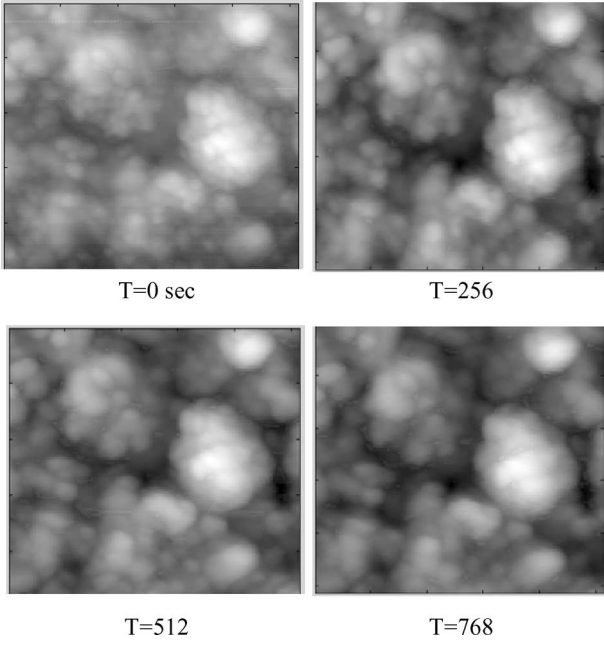


Fig. 9. Image sequences of a graphite sample by an AFM tapping mode taken at 256 s intervals with drift compensation. The scanned area is $512 \times 512 \text{ nm}^2$.

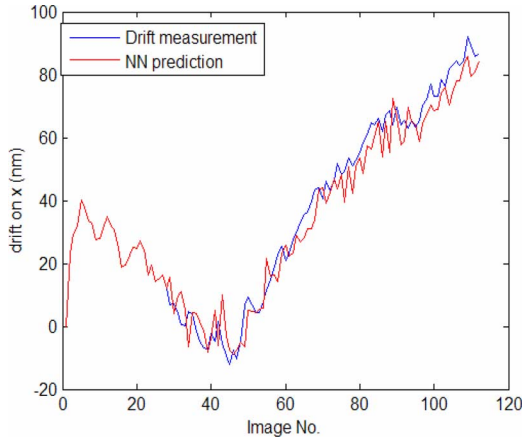


Fig. 10. Measured and predicted drift value from the phase correlation algorithm and the predicted value from the NN.

of the NN predictor and the signal reconstruction block. Fig. 10 displays the errors between the measured and the predicted drift values along the x -direction, which average at 1.62 nm with a peak of 6.88 nm. In Fig. 11, we can see the continuous function of the drift after the signal reconstruction process.

In the end, to evaluate the effectiveness of our algorithm under the influence of manipulation, which is one of the major contributions of our paper, the compensator is implemented for an automatic manipulation task. Fig. 12 depicts the results of manipulating gold particles with 30 nm of diameter on a mica substrate. One of the particles is manipulated to form a line with two other particles, and the other is moved out of the screen. The drift measurement and the compensation are finished before starting the manipulation routines.

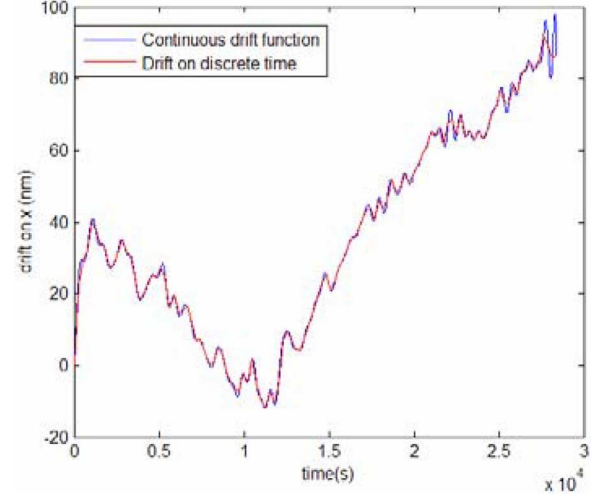


Fig. 11. Continuous drift function after the signal reconstruction compared with the discrete drift measurement.

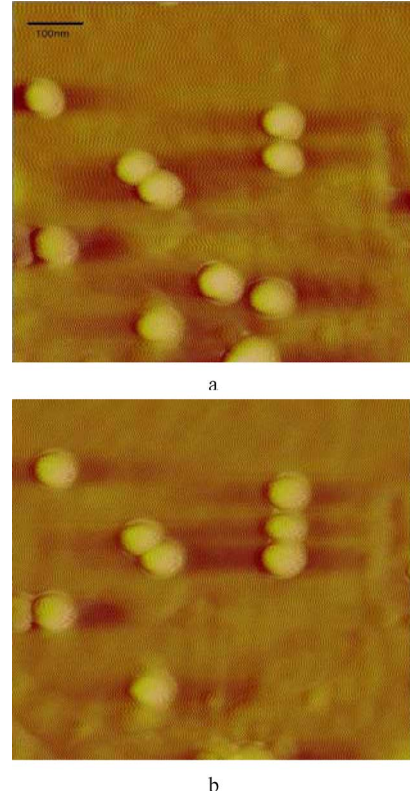


Fig. 12. Manipulation of 30 nm gold particles using the block-based phase correlation compensator.

V. CONCLUSION AND FUTURE WORK

To realize fully automated nanomanipulation and nanofabrication, the effects of nonlinearity and spatial uncertainties of AFMs have to be compensated in order to minimize user intervention. This paper describes a novel compensation system for drift, which is a major cause of spatial uncertainty. The compensating scheme can be subsequently used in designing a real-time controller for nanomanipulation. Experimental results show that

the proposed scheme is able to predict drift that can be successfully utilized for compensation during nanomanipulation.

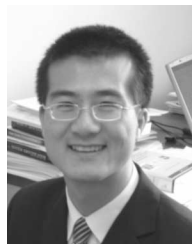
As part of future work, similar to the drift compensation, more efficient tools must be developed for other uncertainties, such as creep, hysteresis, etc. Trying other prediction methodologies to lower the tracking errors is also our future work. Moreover, since the microscope undergoes drift simultaneously as capturing images, fundamentally speaking, any images obtained from the AFM are drift "contaminated." To eliminate the drift error within an image, possible solutions in the future will include: 1) updating the current image by using the force feedback from the microscope during manipulation; 2) using smaller imaging area for reducing the drift within one image; and 3) using multiple tips and conduct manipulation and drift compensation simultaneously in a parallel way.

ACKNOWLEDGMENT

The authors thank the anonymous reviewers for their helpful comments.

REFERENCES

- [1] D. M. Eigler and E. K. Schweizer, "Positioning single atoms with a scanning electron microscope," *Nature*, vol. 344, pp. 524–526, 1990.
- [2] M. Sitti, "Survey of nanomanipulation systems," in *Proc. 1st IEEE Conf. Nanotechnol.*, 2001, pp. 75–80.
- [3] B. Mokaberi and A. A. G. Requicha, "Towards automatic nanomanipulation: Drift compensation in scanning probe microscopes," in *Proc. IEEE Int. Conf. Robot. Autom.*, 2004, vol. 1, pp. 416–421.
- [4] V. Y. Yurov and A. N. Klimov, "Scanning tunneling microscope calibration and reconstruction of real image: Drift and slope elimination," *Rev. Sci. Instrum.*, vol. 65, no. 5, pp. 1551–1557, 1994.
- [5] R. Staub, D. Allia, and C. Nicolini, "Drift elimination in the calibration of scanning probe microscopes," *Rev. Sci. Instrum.*, vol. 66, no. 3, pp. 2513–2516, 1995.
- [6] J. T. Woodward and D. K. Schwartz, "Removing drift from scanning probe microscope images of periodic samples," *J. Vac. Sci. Technol. B*, vol. 16, no. 1, pp. 51–53, 1998.
- [7] S. H. Huerth and H. D. Hallen, "Quantitative method of image analysis when drift is present in a scanning probe microscope," *J. Vac. Sci. Technol. B*, vol. 21, no. 2, pp. 714–718, 2003.
- [8] K. J. Ito, Y. Uehara, S. Ushioda, and K. Ito, "Servomechanism for locking scanning tunneling microscope tip over surface nanostructures," *Rev. Sci. Instrum.*, vol. 71, no. 2, pp. 420–423, 2000.
- [9] C. Stiller and J. Konrad, "Estimating motion in image sequences," in *Proc. IEEE Signal Mag.*, 1999, pp. 70–91.
- [10] G. Li, N. Xi, H. Chen, C. Pomeroy, and M. Prokos, "'Videolized' atomic force microscopy for interactive nanomanipulation and nanoassembly," *IEEE Trans. Nanotechnol.*, vol. 4, no. 5, pp. 605–615, Sep. 2005.
- [11] W. Vogl, B. Ma, and M. Sitti, "Augmented reality user interface for an atomic force microscope based nanorobotic system," *IEEE Trans. Nanotechnol.*, vol. 5, no. 4, pp. 397–406, Jul. 2006.
- [12] M. Sitti and H. Hashimoto, "Teleoperated touch feedback of surfaces at the nanoscale: Modeling and experiments," *IEEE/ASME Trans. Mechatron.*, vol. 8, no. 2, pp. 287–298, Jun. 2003.
- [13] A. A. G. Requicha, "Nanorobots, NEMS and nanoassembly," *Proc. IEEE*, vol. 91, no. 11, pp. 1922–1933, 2003.
- [14] Q. Yang and S. Jagannathan, "Atomic force microscope-based nanomanipulation with drift compensation," *Int. J. Nanotechnol.*, vol. 3, no. 4, pp. 527–544, 2006.
- [15] M. Sitti and H. Hashimoto, "Controlled pushing of nanoparticles: Modeling and experiments," *IEEE/ASME Trans. Mechatron.*, vol. 5, no. 2, pp. 199–211, Jun. 2000.
- [16] J. E. Griffith and D. A. Grigg, "Dimensional metrology with scanning probe microscopes," *J. Appl. Phys.*, vol. 74, pp. R83–R109, 1993.
- [17] B. Mokaberi and A. A. G. Requicha, "Drift compensation for automatic nanomanipulation with scanning probe microscopes," *IEEE Trans. Autom. Sci. Eng.*, vol. 3, no. 3, pp. 199–207, Jul. 2006.



Qinmin Yang (S'05) was born in Hengyang, China, in 1979. He received the Bachelor's degree from the College of Electrical and Information Engineering, Civil Aviation University of China, Tianjin, China, in 2001, the M.S. degree from the Institute of Automation, Chinese Academy of Sciences, Beijing, China, in 2004, and the Ph.D. degree from the University of Missouri-Rolla, Rolla, in 2007, all in electrical engineering.

He is currently a Postdoctoral Research Associate at the University of Missouri-Rolla. His current research interests include intelligent control, neural network learning, nanorobotics, autonomous systems/mobile robotics, and system diagnosis.



S. Jagannathan (M'95–SM'99) received the Bachelor's degree from the College of Engineering, Guindy at Anna University, Chennai, India, the M.S. degree from the University of Saskatchewan, Saskatoon, Canada, and the Ph.D. degree from the University of Texas, Austin, in 1994.

During 1986–1987, he was with Engineers India Limited, New Delhi, India, as a Junior Engineer. From 1990 to 1991, he was with the University of Manitoba, Winnipeg, Canada, as a Research Associate and an Instructor. During 1994–1998, he was with Caterpillar, Inc., Peoria, IL, where he worked at the Systems and Controls Research Division, as a Consultant. During 1998–2001, he was with the University of Texas. Since September 2001, he has been with the University of Missouri-Rolla, Rolla, where he is currently a Professor and the Site Director for the National Science Foundation (NSF) Industry/University Cooperative Research Center on Intelligent Maintenance Systems. He is the author or coauthor of more than 180 refereed conference and journal articles, and several book chapters. He is also the coauthor of the books *Neural Network Control of Robot Manipulators and Nonlinear Systems* (Taylor & Francis, 1999), *Discrete-Time Neural Network Control of Nonlinear Discrete-Time Systems* (CRC Press, April 2006), and *Wireless Ad Hoc and Sensor Networks: Performance, Protocols and Control* (CRC Press, April 2007). His current research interests include adaptive and neural network control, computer/communication/sensor networks, prognostics, and autonomous systems/robotics. He currently holds 17 patents and several are in process.

Prof. Jagannathan received several gold medals and scholarships during his undergraduate program. He was the recipient of the Region 5 IEEE Outstanding Branch Counselor Award in 2006, the Faculty Excellence Award in 2006, the St. Louis Outstanding Branch Counselor Award in 2005, the Teaching Excellence Award in 2005, the Caterpillar Research Excellence Award in 2001, the Presidential Award for Research Excellence at the University of Texas at San Antonio (UTSA) in 2001, the NSF CAREER award in 2000, the Faculty Research Award in 2000, the Patent Award in 1996, and the Sigma Xi "Doctoral Research Award" in 1994. He has served and is currently serving on the program committees of several IEEE conferences. He is also an Associate Editor for the IEEE TRANSACTIONS ON CONTROL SYSTEMS TECHNOLOGY, the IEEE TRANSACTIONS ON NEURAL NETWORKS, the IEEE TRANSACTIONS ON SYSTEMS ENGINEERING, and also for several program committees. He is a member of the Tau Beta Pi, Eta Kappa Nu, Sigma Xi, and the IEEE Committee on Intelligent Control. He is currently the Program Chair for the 2007 IEEE International Symposium on Intelligent Control and the Publicity Chair for the 2007 International Symposium on Adaptive Dynamic Programming.



E. W. Bohannon was born in Waynesville, MO, in 1969. He received the Bachelor's degree in chemistry with a minor in biology from Truman State University, Kirksville, MO, in 1993, and the Ph.D. degree in chemistry from the University of Missouri-Rolla, Rolla, in 1999.

He is currently a Research Assistant Professor in the Materials Science and Engineering Department and a Senior Research Specialist at the Graduate Center for Materials Research, University of Missouri-Rolla. His current research interests include electrochemistry, chiral electrodeposition, epitaxial electrodeposition, and environmental chemistry.